

Studying the gaseous outskirts of galaxy groups with coherent Ly α absorption patterns ^{*}

P. Richter¹, J.C. Charlton², A.J. Fox³, Sameer^{4,2} and B.P. Wakker⁵

¹ Institut für Physik und Astronomie, Universität Potsdam, Karl-Liebknecht-Str. 24/25, 14476 Golm, Germany

² Department of Astronomy & Astrophysics, 525 Davey Lab, The Pennsylvania State University, University Park, PA 16802, USA

³ AURA for ESA, Space Telescope Science Institute, 3700 San Martin Drive, Baltimore, MD 21218, USA

⁴ Department of Physics & Astronomy, Nieuwland Science Hall, The University of Notre Dame, Notre Dame, IN 46556, USA

⁵ Eureka Scientific, Inc., 2452 Delmer Street, Oakland, CA 94602, USA

Received 23 November 2024; accepted 15 July 2025

ABSTRACT

Aims. In this study, we explore the properties of diffuse intergalactic gas residing in the outskirts of the four nearby, low-mass galaxy groups NGC 1052, NGC 5866, NGC 4631, and NGC 3992 (all at $cz \leq 2000 \text{ km s}^{-1}$) beyond their group virial radii.

Methods. Using archival ultraviolet absorption spectra of bright active galactic nuclei (AGN) observed with the *Hubble Space Telescope* (HST) and its Cosmic Origins Spectrograph (COS), we search for H I Ly α absorption near the group's recession velocities along 35 sightlines that pass the outer group medium (OGrM) at normalized impact parameters $\rho/R_{\text{vir}} = 1 - 3$. We derive H I column densities of the absorbers and constrain the physical conditions in the gas (thermal pressure, density, neutral gas fraction, absorption path-length) by using a hydrostatic toy model of the group's gas environment and assuming photoionization.

Results. H I Ly α absorption near the group's recession velocities is detected along 19 sightlines with H I column densities in the range $\log(N(\text{H I})/\text{cm}^{-2}) = 12.50 - 14.34$, implying a high OGrM detection rate of more than 50 percent. We transform this value into an incidence rate of OGrM absorbers per unit redshift of $dN/dz = 232 \pm 58$ for absorbers with $\log(N(\text{H I})/\text{cm}^{-2}) \geq 13.2$ and $\rho/R_{\text{vir}} = 1 - 3$. This is 25 percent above the value derived for the general population of Ly α absorbers within $z = 0$ filaments and more than twice the value for the $z = 0$ Ly α forest (considering the same column-density range). From the modeling, we obtain lower limits for the gas densities from $\log(n_{\text{H}}/\text{cm}^{-3}) = -5.00$ to -3.72 , comparable to densities found in the overall Ly α forest.

Conclusions. Our study unveils a large cross section and overdensity of Ly α absorbers in the outskirts of these four nearby groups. Such an overdensity is in line with a previously proposed scenario, in which AGN feedback lifts gaseous material to large distances beyond the virial radius of groups into the OGrM. However, a larger survey of OGrM absorbers and a comparison with hydrodynamical simulations will be necessary to constrain the cosmological mass density of OGrM absorbers and pinpoint their role in cosmological structure formation and galaxy/group evolution.

1. Introduction

Galaxy groups in the mass range $M = 10^{12} - 10^{14} M_{\odot}$ represent particularly representative cosmological structures in the Universe, as they harbor the majority of the star-forming galaxies in the Universe (Mulchaey, 2000; Eke et al., 2006; Lovisari et al., 2021). In addition, the Dark Matter (DM) halo mass function at low redshift peaks in this mass range (e.g., Despali, Giocoli & Tormen, 2014). In the canonical picture of the Universe's large-scale structure, such low-mass galaxy group environments represent mildly overdense matter knots in the filamentary Cosmic Web (Tempel et al., 2014). In contrast to more massive groups and clusters, the intra-group medium (IGrM) in low-

mass groups is too cold (and too diffuse) to be detectable in X-ray emission throughout the overall group environment (Mulchaey et al., 1996). This leaves absorption-line spectroscopy against bright AGN as the only efficient method to systematically explore the diffuse, multi-phase IGrM with a particular focus on H I Ly α /Ly β and, potentially, low, intermediate and high metal ions such as C II, Mg II, Si III, Si IV, C IV, and O VI (Savage et al., 2014; Stocke et al., 2014; Richter et al., 2016; Bielby et al., 2017; Sameer et al., 2022). Recent absorption-line studies of individual group environments unveil absorber properties and absorber/galaxy relations that differ from those in isolated galaxy environments (Stocke et al., 2019; Pointon et al., 2017, 2020), reflecting the on-going cosmological structure formation in these overdense regions. Star-formation activity, triggered by gas-accretion processes in groups, will lead to outflows and winds, depositing energy and heavy elements in the IGrM that can be detected by measuring high-ion absorption (e.g., from C IV and O VI) along sightlines that pass group environments (e.g., Burchett et al., 2018; Stocke et al., 2019; Sameer et al., 2022). Other case studies of pre-

Send offprint requests to: P. Richter

e-mail: prichter@astro.physik.uni-potsdam.de

^{*} Based on observations obtained with the NASA/ESA Hubble Space Telescope, which is operated by the Space Telescope Science Institute (STScI) for the Association of Universities for Research in Astronomy, Inc., under NASA contract NAS5D26555.

Table 1. Group parameters

| Group name | Alt. group names ^a | α_{2000} ^b [deg] | δ_{2000} ^b [deg] | D ^c [Mpc] | v_{gr} ^d [km s ⁻¹] | N_{gal} ^e | \log (M_{dyn}/M_{\odot}) ^f | \log (M_L/M_{\odot}) ^g | R_{vir} [Mpc] | σ_v ^h [km s ⁻¹] |
|----------------|-------------------------------|---------------------------------------|---------------------------------------|---------------------------|--|------------------------|--|--|--------------------|--|
| NGC 1052 group | LGG 71 | 40.107 | -7.883 | 19 | 1240 – 1540 | 9 | 12.42 | 12.66 | 0.45 | 105.7 |
| NGC 5866 group | LGG 396 | 228.368 | 56.250 | 16 | 650 – 850 | 5 | 12.09 | 12.34 | 0.35 | 82.0 |
| NGC 4631 group | LGG 291, Coma I | 187.645 | 30.372 | 9 | 520 – 820 | 12 | 12.36 | 12.62 | 0.43 | 100.5 |
| NGC 3992 group | UMaIN, LGG 258 | 177.431 | 53.648 | 20 | 640 – 1280 | 32 | 13.03 | 13.27 | 0.72 | 168.3 |

^a see, e.g., Fouqué et al. (1992) and Garcia (1993); ^b luminosity-weighted group center coordinate; ^c distance adopted from NED; ^d group’s radial velocity range (see Sect. 2.2); ^e number of bright member galaxies (from Fouqué et al., 1992). ^f dynamical mass; ^g luminosity-based mass; ^h velocity dispersion from group member galaxies.

selected group environments with multi-wavelength observations demonstrate that galaxy mergers have a crucial influence on the large-scale properties of the IGrM (Yun, Ho & Lo, 1994; Borthakur, Yun & Verdes-Montenegro, 2010; Richter et al., 2018). This is supported by zoom-in cosmological simulations of groups, which demonstrate that the covering fraction of high-column density gas in the IGrM rises substantially in the time-frame of merger events, leaving their imprints in the cross-section of intermediate and high ions (see Oppenheimer et al. 2021 and references therein). Characterizing the gas-circulation processes in the IGrM around galaxies as a function of their immediate cosmological environment therefore is of fundamental importance to understand cosmological structure-formation.

So far, very little attention has been paid in the literature to absorption signatures of gas in the outskirts of low-mass galaxy groups beyond the group’s virial radius (and beyond the virial radius of group member galaxies), where the groups connect to the Cosmic Web. As recent studies imply, the gaseous outskirts of groups are believed to host a substantial amount of baryons in the form of warm/hot gas, a direct result of AGN feedback that potentially lifts gaseous material to large distances even beyond the group’s virial radii (see Eckert et al., 2021, and references therein). From this reservoir, group member galaxies can accrete metal-poor gas to fuel star formation, making this gas component particularly interesting for our understanding of galaxy evolution. In this interface region between the IGrM and the ambient filamentary IGM, the mean gas density is expected to be very low (close to that of the IGM itself) where $n_H < 10^{-4} \text{ cm}^{-3}$, typically (Martizzi et al., 2019). As a result, metal absorption is expected to be very rare, leaving HI Ly α absorption as the only sensitive tracer of this gas, which we hereafter refer to as outer-group medium (OGrM). Note that, in this definition, OGrM Ly α absorbers represent a sub-class of Ly α filament absorbers (e.g., Wakker et al., 2015; Bouma, Richter & Wendt, 2022) and the overall Ly α forest (e.g., Lehner et al., 2007; Danforth et al., 2016), as groups and their gaseous environment represent galaxy overdensities within the hierarchically-structured Cosmic Web. As the OGrM is expected to be gravitationally coupled to the group’s DM potential, OGrM absorbers are expected to cluster around the group’s recession velocity/redshift. This is possibly separating them from “free-floating” absorption systems within the Cosmic Web or in voids that do not have such a clear kinematic association with galaxy concentrations.

The above considerations motivated us to start a systematic search for OGrM HI Ly α absorption features in archival HST/COS spectra along sightlines that pass nearby galaxy groups and analyze their properties. In this pilot study, we present our results for four nearby

galaxy groups at recession velocities $cz \leq 2000 \text{ km s}^{-1}$: the NGC 1052 group, the NGC 5866 group, the NGC 4631 group, and the NGC 3992 group.

This paper is organized as follows: in Sect. 2, we present the search strategy, the data basis and handling and the analysis method. In Sect. 3, we discuss the individual OGrM absorbers and their relation to the groups. The properties of the absorbers and the physical conditions in the gas are discussed in the Sect. 4. A summary of our study as well as final conclusions are presented in Sect. 5. The appendix provides additional information on the continuum-fitting process and the hydrostatic toy model.

2. Data handling and analysis method

2.1. Search strategy

To study diffuse gas in the large-scale environment of nearby galaxy groups, we have combined archival ultraviolet (UV) spectral data from HST/COS with publicly available galaxy data and information from various galaxy-group surveys.

As spectral data basis, we used 1040 COS G130M+G160M data sets of distant ($z > 0.01$) AGN and galaxies downloaded from the MAST archive, as available to us by February 2025. For this, we used the data selection strategy outlined in our previous HST/COS archival surveys (Richter et al., 2016, 2017). Since we are aiming at studying the HI Ly α absorption signatures of very nearby (in a cosmological sense) galaxy groups at recession velocities $cz \leq 5000 \text{ km s}^{-1}$, we have pre-selected those 311 AGN spectra that have a signal-to-noise ratio of $S/N \geq 6$ per 17 km s^{-1} wide spectral resolution element of COS at 1230 \AA . This S/N cutoff was chosen because of the fact that it becomes very difficult to unambiguously identify weak absorption features in the extended wing of the Galactic interstellar Ly α absorption at S/N ratios < 6 . We also do not consider those spectra, for which the flux distribution in the red wing of the interstellar Ly α absorption is highly irregular (so that a reliable reconstruction of the continuum is not possible) or that exhibit a critical number of blending lines at $\lambda = 1220 - 1230 \text{ \AA}$ from other systems at higher redshift.

To identify $z \approx 0$ galaxy groups that lie in the vicinity of the pre-selected archival HST/COS AGN sightlines, we used the classical group catalog of very nearby ($cz \leq 6000 \text{ km s}^{-1}$) galaxy groups and their brightest member galaxies from Fouqué et al. (1992) to calculate the group’s mass and radial extent (see Sect. 2.2). For each group listed in this catalog, we created finding charts by cross-correlating the positions of the COS AGN with the group’s positions in an impact-parameter range between $1 - 3 R_{vir}$. In this

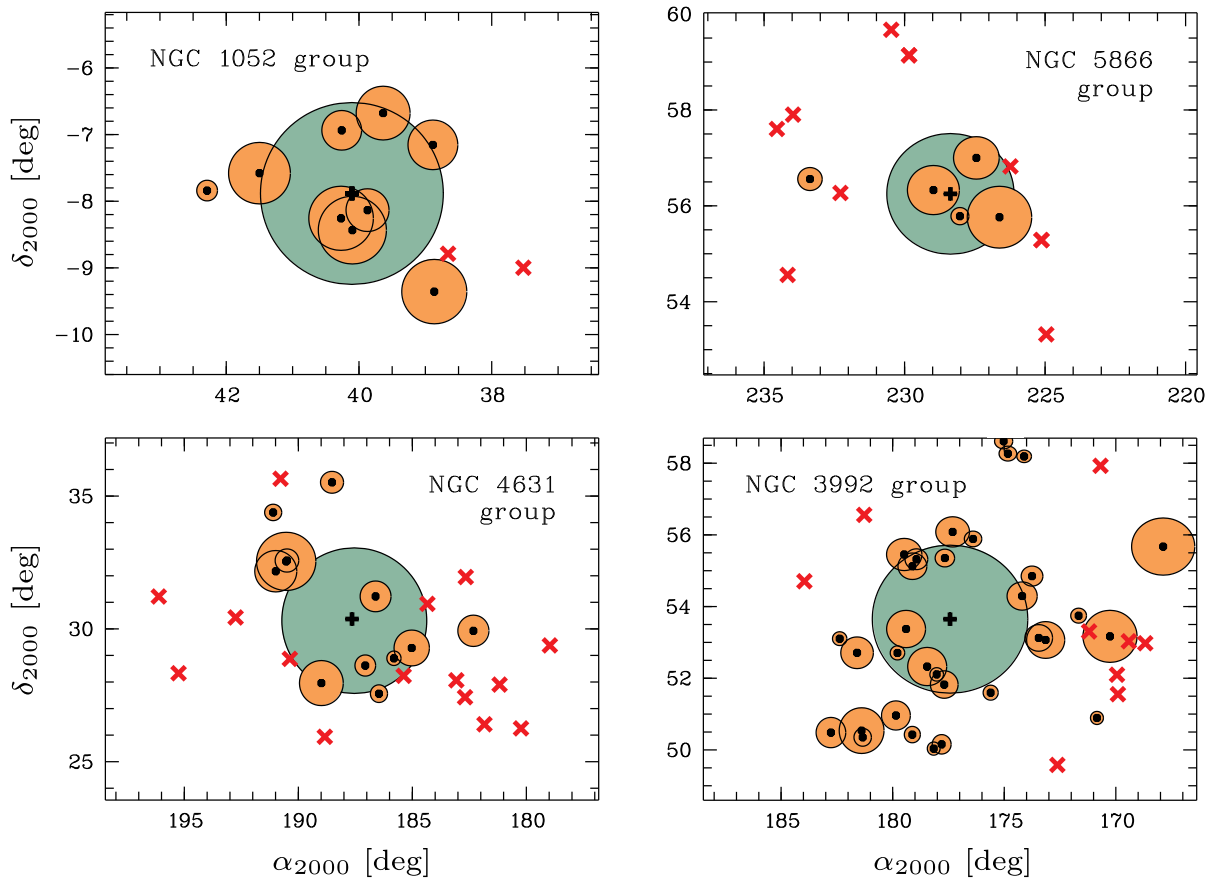


Fig. 1. Spatial distribution of the galaxies in the NGC 1052, NGC 5866, NGC 4631, NGC 3992 galaxy groups together with the galaxies’ (orange-shaded circles) and groups’ (green-shaded circles) virial radii and the position of the selected background AGN sampled by HST/COS data (red crosses).

way, we identified outer-group environments at $cz \leq 5000$ km s^{-1} that are sampled by at least two AGN sightlines. All in all, we have identified 14 galaxy groups in this manner whose OGrM can be studied in HI Ly α absorption with archival HST/COS data.

In this study, we focus on four particularly interesting nearby group environments at $cz \leq 2000$ km s^{-1} : the NGC 1052 group, the NGC 5866 group, the NGC 4631 group, and the NGC 3992 group. Throughout the following, we use the group names from the original work by Fouqué et al. (1992) except for group labeled as "Ursa Major I North group" in Fouqué et al. (1992), for which we use the alternative name "NGC 3992 group" to avoid confusion with the labeling of Ursa Major group environments used in other group catalogues (see Wolfinger et al., 2016). The "NGC 4631 group" is also known under the name "Coma I group" and the circumgalactic environment of NGC 4631 itself previously has been studied by us using UV absorption-line data from HST/COS in combination with HI 21cm from the HALOGAS survey (Richter et al., 2018). Alternative group names are listed in Table 1, second column.

Based on our HST/COS archival data set and the above-mentioned selection criteria, we identify 56 HST/COS spectra that sample the outer environment of these four groups in the range $\rho/R_{\text{vir}} = 1 - 3$. From these, however, 21 sightlines exhibit Ly α absorption that we associate with the circumgalactic medium (CGM) of group-member galaxies or foreground galaxies, as discussed in Sect. 2.3. Therefore, our

final, CGM-corrected spectral sample consists of 35 AGN sightlines that can be used to study the OGrM of these four groups.

Some of these AGN have been observed by COS at a relatively high S/N of > 20 per resolution element, so that very weak HI Ly α absorbers at column densities $N(\text{HI}) \leq 10^{13} \text{ cm}^{-2}$ can also be detected. These four groups, together with the rich HST/COS data set, therefore represent an ideal starting point for a sensitive first systematic study of the OGrM in Ly α absorption. In Table 1, we summarize the main properties of the NGC 1052, NGC 5866, NGC 4631, and NGC 3992 groups.

2.2. Group parameters and galaxy data

For our study, we use the group catalog from Fouqué et al. (1992), which is particularly strict in defining group members. In this catalog, only the largest group member galaxies with isophotal diameters $D_{25} \geq 100^1$ arcsec are considered, which contain most of the stellar mass and luminosity of these groups. As described in Gourgoulhon, Chamaroux & Fouqué (1992), the group members were identified using a hierarchical finding algorithm, where the hierarchy is built on the mass density of the aggregates progressively formed by the algorithm. Only those galaxy aggregates are

¹ D_{25} is the isophotal diameter measured at a surface brightness of 25 magnitudes per square arcsecond.

considered that have a B-band luminosity density higher than $8 \times 10^9 L_\odot \text{Mpc}^{-3}$, ensuring that the group is gravitationally bound. In addition, the galaxy-selection criterion, together with the hierarchical method, warrants that contamination with field galaxies and due to projection effects with filaments is minimized (see discussion in Gourgoulhon, Chamaraux & Fouqué, 1992). The latter two aspects are particularly important for our study, as we use the kinematic information on the confirmed members galaxies to define the search window for Ly α absorption associated with the groups and separate the OGrM absorber statistics from that of “field”/filament Ly α absorbers (Danforth et al., 2016; Bouma, Richter & Wendt, 2022; Wakker et al., 2015).

Galaxy data for the 58 confirmed group members (as listed in Fouqué et al., 1992, see Table 1, 7th column) and for other, potential group member galaxies that are spatially and kinematically aligned with the four groups have been extracted from the NED and SIMBAD online data bases. These data include J2000 coordinates, B-band magnitudes, distances, and radial velocities for a total of 430 galaxies in the four group fields displayed in Fig. 1. Since all these galaxies are very nearby ($D \leq 20$ Mpc), we estimate that our galaxy sample is complete down to luminosities of $\sim 0.08 L^*$ (see French & Wakker, 2017, their Fig. 1).

For the group member galaxies, we have derived B-band luminosities and virial radii (R_{vir}) of the galaxies using the scaling relation from Richter et al. (2016, their equation (3)), which is based on the approach described in Stocke et al. (2013). From the positions of the galaxies, we have then calculated the luminosity-weighted group center coordinates, as given in Table 1 (columns 3 & 4). For each of the four groups, we then derived the velocity dispersion of the group member galaxies using the relation from Osmond & Ponman (2004),

$$\sigma_v = \sqrt{\frac{\sum (v - \bar{v})^2}{N_{\text{gal}} - 3/2}} \pm \frac{\sigma_v}{\sqrt{2(N_{\text{gal}} - 3/2)}}, \quad (1)$$

where N_{gal} denotes the number of group members, v is the velocity of each individual group member, and \bar{v} is the mean galaxy velocity in the group. For the determination of the *dynamical* mass of each group (Table 1, 8th column), we have used the relation of Tully (2015),

$$\frac{M_{\text{dyn}}}{M_\odot} = 1.5 \times 10^6 h^{-1} \left(\frac{\sigma_v}{\text{km s}^{-1}} \right)^3, \quad (2)$$

where we have to assume the groups to be virialized. For low-mass groups, however, the latter assumption may not hold (e.g. Marini et al., 2024), introducing a substantial systematic uncertainty in the determination of the dynamical group mass.

An alternative way to determine the mass of low-mass groups is to consider the group’s total luminosity (see discussion in Marini et al., 2024). To do this, we use the luminosity-to-mass conversion scheme presented in Stocke et al. (2019, their equation (4)) together with a group mass-to-light ratio of $\Upsilon_{\text{grp}} = M_{\text{grp}}/L_{\text{grp}} = 150$, as appropriate for groups with total luminosities $\log(L_{\text{grp}}/L_\odot) \leq 11.2$ (Proctor et al., 2015), to define

$$\frac{M_L}{M_\odot} = \Upsilon_{\text{grp}} 10^{10} \left(\frac{L_{\text{grp}}}{L^*} \right). \quad (3)$$

The luminosity-based group masses, M_L , derived in this way are listed in Table 1, 9th column. As can be seen, the values for M_L are slightly higher than for M_{dyn} (~ 0.25 dex), possibly related to the fact that these groups are not (yet) fully virialized. For the following, we therefore use M_L as a measure for the groups’ total masses.

To characterize the groups’ radial extent, we have calculated R_{vir} for each group under the assumption that their potentials follow an NFW profile (Navarro, Frenk & White, 1995). For this, we have used the relation (A1) given in Richter (2020), which is based on the work by Maller & Bullock (2004), where we assume a virial overdensity of $\Delta_{\text{vir}} = 360$ at the virialization redshift of $z = 0$ (see also Shull, 2014).²

While we do not use the data for the other galaxies in the group fields to determine group masses and virial radii (as their group-membership status is unclear), we do consider these galaxies in Sect. 3 to identify (and sort out) CGM absorbers that arise in the halos of these “field” galaxies.

In Fig. 1, we display the spatial distribution of the galaxies in the four groups together with the member galaxies’ R_{vir} and the groups’ virial radii. The positions of the background AGN are indicated with red crosses.

2.3. COS data and their spectral analysis

The overall strategy of the data reduction and analysis method of the HST/COS data follows the approach that we have used in our previous surveys and studies involving HST/COS spectral data (e.g., Richter et al., 2016, 2017; Richter, 2020). The original (raw) data of the individual COS science exposures (from the G130M and G160M gratings) of the AGN sample available to us were processed by the CALCOS pipeline (v3.4.3) and transformed into standard x1d fits files. In a second step, the individual exposures then were coadded using a custom-written code that aligns individual exposures based on a pixel/wavelength calibration (see Richter et al., 2017, for a detailed description).

For our study of HI Ly α absorption in the OGrM in nearby groups at $cz \leq 2000$ km s $^{-1}$, the relevant wavelength range is 1215.67 – 1223.78 Å. This short wavelength interval is covered by the COS G130M grating, which operates from 1150 – 1450 Å at a spectral resolution of $R \approx 15,000 - 18,000$ ($\approx 20 - 17$ km s $^{-1}$ FWHM), depending on wavelength, central wavelength setting, and the lifetime position of the COS detector. The native pixel size in the data is 3 km s $^{-1}$ (Green et al., 2012; Debes, Becker & Roman-Duval, 2016). With this targeted wavelength range, the OGrM Ly α absorption is expected to arise in the red wing of the damped interstellar Ly α absorption trough (centered near 1215.67 Å), which typically reaches out to $\lambda = 1220 - 1227$ Å depending on the local HI column density in the direction of the background

² Note that in the context of galaxy groups and clusters, their characteristic radius often is expressed in terms of r_{200} , the radius for which the mass density profile of a halo equals 200 times the critical density of the Universe; at $z = 0$, $R_{\text{vir}} > r_{200}$ and $R_{\text{vir}} \approx r_{100}$ (Bryan & Norman, 1998).

AGN. Therefore, each COS spectrum used in this study was carefully continuum normalized in the 1215 – 1230 Å range using the custom-written spectral analysis code `span` (Richter et al., 2013) together with a Voigt-profile model of the foreground Milky Way interstellar Ly α absorption. An example for the continuum reconstruction of the interstellar Ly α trough towards NGC 985 is presented in the Appendix in Fig. A.1.

As mentioned above, a significant fraction of the sightlines in our original sample of 56 HST/COS spectra passes the immediate environment of group member galaxies or foreground galaxies, possibly tracing their CGM rather than the OGrM of the group. As criterion for a positive CGM Ly α detection, we require that the sightline passes a galaxy at an impact parameter $\rho \leq R_{\text{vir}}$ with the absorption arising within $\pm 500 \text{ km s}^{-1}$ of the galaxy’s systemic velocity. We find 21 such cases in our sample and remove these sightlines from our analysis, which leaves 35 sightlines for the OGrM analysis (Table 2). Note that sightlines that do pass a galaxy at $\rho \leq R_{\text{vir}}$ and that do not exhibit Ly α absorption in the galaxy’s or group’s velocity range still indicate a significant non-detection for OGrM absorption in our sample.

In the next step, we scanned the remaining 35 COS spectra for intervening absorption features that potentially could represent H I Ly α absorption arising in the extended OGrM of these groups. For this, we consider a velocity range $\Delta v_{\text{abs}} = \Delta v_{\text{gal}} \pm 150 \text{ km s}^{-1}$, where Δv_{gal} is the observed velocity range of the group member galaxies listed in Table 1, sixth column. Ly α -forest absorbers that are unrelated to the group and its environment could also coincidentally fall in this velocity range, however. This aspect needs to be taken into account because the line density of the Ly α forest at $z = 0$ is substantial, the number of Ly α absorbers per unit redshift dN/dz being ≈ 100 for $\log N(\text{H I}) \geq 13.2$ (Lehner et al., 2007; Danforth et al., 2016). Since $v = cz$ at $z = 0$, this line density implies that the likelihood of a randomly placed Ly α absorber in a low- z AGN spectrum to coincidentally fall into a pre-defined velocity interval of width $\Delta v = 500 \text{ km s}^{-1}$ is non-negligible, namely ~ 0.17 . The likelihood for a double-coincidence absorption in the same velocity interval along two adjacent lines of sight (LOS) is much smaller, however, ~ 0.03 . To minimize the contamination by coincidental Ly α absorbers in our OGrM sample, we therefore consider Ly α absorbers within Δv_{abs} as OGrM candidates only if i) they have at least one neighboring sightline with Ly α absorption in the same group velocity interval and ii) their absorption-velocity ranges overlap with each other. In this way, we expect OGrM absorbers to form a Ly α “coherence pattern” along adjacent sightlines (as they align in position and velocity, similar as the group member galaxies). Similar considerations on random and non-random coincidences of Ly α absorbers have been used to study the coherence length of IGM structures against AGN pairs (e.g. Dinshaw et al., 1997).

For each detected OGrM Ly α candidate line, we measured the radial velocity and equivalent width (EW) using the `span` code and cross-checked whether it could be a metal line or higher H I Lyman-series lines from other intervening absorption systems at higher redshift. We did not find, however, convincing alternative identifications for any of the detected absorption features, supporting the conclusion that they indeed represent H I Ly α absorption lines.

For the subsequent analysis, we used the component-modeling method implemented in `span` to derive column densities, $\log N(\text{H I})$, and Doppler parameters (b values) for each resolved absorption component. In Fig. A.1, we show as an example the modeled Ly α OGrM absorber at 1222.6 Å towards NGC 985. For those absorbers, for which the absorber shape is uncertain (either due to particularly weak or particularly strong absorption), we apply the apparent optical depth (AOD) method (Savage & Sembach, 1991) to obtain $\log N(\text{H I})$ (or limits thereof) from a direct pixel integration (without gaining information on b). Throughout the paper, we give column densities in units $[\text{cm}^{-2}]$, particle densities in units $[\text{cm}^{-3}]$, and temperatures in units [K]. All results from the absorption-line measurements and component modeling are summarized in Table 3.

The main properties of the 35 background AGN and the S/N in the COS data are listed in Table 2. Instead of using the AGN names used in the COS archive, we here list the most appropriate AGN names (based on the NED/SIMBAD entries) in the second column of Table 2 with alternative names in parentheses.

3. Discussion of individual absorbers

3.1. General absorber statistics

In the final sample of 35 AGN spectra, H I Ly α absorption within the groups’ velocity range Δv_{abs} (gray shaded area in the velocity plots in Figs. 2-5) is detected along 19 sightlines (Table 3). Only one of these OGrM absorbers (towards Ton 133) possibly has associated metal absorption (Si III; see Sect. 3.4), so that the vast majority of the systems are considered as “Ly α -only absorbers” (but see also Muzahid et al., 2018, for a potential group-related population of weak metal absorbers). In Sects. 3.2-3.5, we discuss the properties of the absorbers individually for each group environment.

With these numbers, it is already evident that OGrM absorbers are frequent; the detection rate comes out to $f_{\text{det}} = 19/35 = 0.54$. More meaningful is the detection rate for a (minimum) limiting H I column density, N_{lim} , and a pre-defined range in impact parameter. For $\log N_{\text{lim}} = 13.2$ and $\rho/R_{\text{vir}} = 1 - 3$, we have 34 sightlines with a sufficient S/N to detect H I Ly α absorption at that level and 16 OGrM absorbers detected at $\log N(\text{H I}) \geq 13.2$. This implies $f_{\text{det},13.2} = 16/34 = 0.47 \pm 0.12$ for that impact parameter range, the large error being a result of the limited absorber statistics. In Sect. 4.2, we place this detection rate in a cosmological context, by comparing the incidence rate of Ly α absorption in the OGrM with that of Ly α absorption in the local Ly α forest and in nearby filaments.

The measured Ly α equivalent widths in our OGrM absorber sample range from 17 to 505 mÅ, while the logarithmic H I column densities derived from the component-modeling and AOD methods have values of $\log N(\text{H I}) = 12.50 - 14.34$ (see Table 3). This column-density range is very similar to that of the local Ly α forest (Lehner et al., 2007; Danforth et al., 2016; Bouma, Richter & Wendt, 2022, see also Sect. 4.1), implying that these absorbers are predominantly ionized with only small neutral gas fractions. The b values derived from the H I component modeling for the OGrM absorbers lie in the range between 16 and 80 km s^{-1} . Because of the limited spectral resolution and S/N of the COS data, however, the actual component structure

Table 2. List of AGN sightlines tracing OGrM absorption in the four groups

| Group | AGN name(s) ^a | Type ^a | z_{QSO} ^a | α_{2000} ^a [deg] | δ_{2000} ^a [deg] | S/N ^b | |
|--|--|---|-------------------------------|------------------------------------|------------------------------------|------------------|----|
| NGC 1052 | NGC 985 | Seyfert | 0.04314 | 38.657842 | -8.788061 | 57 | |
| | Mrk 1044 | Seyfert | 0.01645 | 37.523011 | -8.998113 | 50 | |
| NGC 5866 | SBS 1537+577 (VV 487, MCG+10-22-028) | Seyfert | 0.07342 | 234.541864 | +57.603645 | 10 | |
| | Mrk 486 (SBS 1535+547) | Seyfert | 0.03900 | 234.160005 | +54.559226 | 10 | |
| | Mrk 290 (SBS 1534+580) | Seyfert | 0.02958 | 233.968346 | +57.902643 | 37 | |
| | SBS 1527+564 (RBS 1503, LEDA 2531253) | Seyfert | 0.09900 | 232.281067 | +56.268536 | 13 | |
| | SBS 1520+598 (SBS 1521+598, 2MASS J1521537+594019) | Seyfert | 0.28620 | 230.474209 | +59.672238 | 10 | |
| | SBS 1518+593 (RBS 1483, LEDA 2816140) | Seyfert | 0.07810 | 229.840292 | +59.139922 | 21 | |
| | SBS 1503+570 (8C 1503+570, RX J1504.8+5649) | Seyfert | 0.35871 | 226.231517 | +56.822315 | 14 | |
| | SBS 1459+554 (RX J1500.5+5517) | Seyfert | 0.40534 | 225.127784 | +55.285886 | 15 | |
| | SBS 1458+534 (LEDA 2437690) | Seyfert | 0.33800 | 224.956648 | +53.319188 | 11 | |
| | NGC 4631 | SDSS J130429.03+311308.2 (CBS 339) | Quasar | 0.80561 | 196.120995 | +31.218966 | 16 |
| SDSS J130100.86+281944.7 (A2 330, CSO 786) | | Quasar | 1.36102 | 195.253615 | +28.329095 | 13 | |
| Ton 133 (CSO 174) | | Quasar | 0.65228 | 192.751299 | +30.428300 | 15 | |
| SDSS J124307.57+353907.1 (CSO 915, LEDA 42770) | | Quasar | 0.54677 | 190.781547 | +35.651971 | 17 | |
| Ton 635 (SDSS J124129.64+285212.0) | | Quasar | 0.58910 | 190.373532 | +28.869996 | 12 | |
| SDSS J123521.58+255613.5 (2XMM J123521.6+255613) | | Seyfert | 0.23993 | 188.839912 | +25.937079 | 10 | |
| WCom (7C 1219+2830) | | BL Lac | 0.10289 | 185.382044 | +28.232917 | 7 | |
| RBS 1090 (CBS 56, FBQS J1217+3056) | | Seyfert | 0.30010 | 184.339236 | +30.941888 | 6 | |
| RX J1212.2+2803 (2MASS J12121725+2803499) | | Seyfert | 0.16758 | 183.071876 | +28.063891 | 12 | |
| RX J1210.7+2725 (SDSS J121045.64+272536.4) | | Seyfert | 0.23010 | 182.690154 | +27.426816 | 15 | |
| RX J1210.6+3157 (7C 1208+3213) | | Seyfert | 0.38891 | 182.656554 | +31.951672 | 9 | |
| SDSS J120720.99+262429.1 (QSO J1207+2624) | | Quasar | 0.32300 | 181.837400 | +26.408100 | 10 | |
| PG 1202+281 (LEDA 38224) | | Seyfert | 0.16530 | 181.175457 | +27.903297 | 9 | |
| RX J1200.9+2615 (SDSS J120056.61+261512.4) | | Seyfert | 0.30801 | 180.235924 | +26.253449 | 14 | |
| SDSS J115552.80+292238.4 (QSO J1155+2922) | | Quasar | 0.51979 | 178.969995 | +29.377345 | 10 | |
| NGC 3992 | | SBS 1213+549 (MCG+09-20-133, RX J1215.8+5442) | Seyfert | 0.15007 | 183.956019 | +54.706660 | 11 |
| | | SDSS J120506.35+563330.9 (ELARS 19) | Galaxy | 0.03087 | 181.276488 | +56.558585 | 5 |
| | Mrk 1447 | Seyfert | 0.09558 | 172.621391 | +49.582726 | 12 | |
| | SDSS J112448.29+531818.8 ([VV2006] J112448.3+531818) | Quasar | 0.53110 | 171.201218 | +53.305237 | 9 | |
| | HS 1119+5812 (SDSS J112244.88+575543.0) | Quasar | 0.90572 | 170.687029 | +57.928637 | 10 | |
| | SBS 1116+523 ([VV2006] J111948.0+520554) | Quasar | 0.35568 | 169.949782 | +52.098045 | 16 | |
| | SBS 1116+518 (RBS 967, RX J1119.6+5133) | Seyfert | 0.10719 | 169.908418 | +51.554311 | 8 | |
| | RX J1117.6+5301 (SDSS J111740.48+530151.2) | Seyfert | 0.15843 | 169.418720 | +53.030904 | 12 | |
| | SDSS J111443.65+525834.2 (2MASX J11144367+5258338) | Seyfert | 0.07908 | 168.681909 | +52.976190 | 8 | |

^a adopted from NED; alternative names are given in parentheses; ^b S/N per resolution element at $\lambda = 1230 \text{ \AA}$.

may not be fully resolved. Therefore, the interpretation of the derived b values (in terms of line-broadening mechanisms) remains afflicted with large uncertainties (see discussion in Sect. 4.1).

In Fig. 2-4, we show velocity plots for the 35 sightlines that pass the OGrM of the four galaxy groups. In the top panel of each figure, we plot the histograms for the radial velocities of the groups' confirmed member galaxies (green) and all galaxies found in these fields (gray). The expected velocity interval for OGrM Ly α absorption is indicated with the gray-shaded range in the velocity plots.

3.2. NGC 1052 group

There are 53 galaxies in the NGC 1052 group field ($\alpha_{2000} \approx 44-36 \text{ deg}$, $\delta_{2000} \approx -11 \text{ to } -5 \text{ deg}$; see Fig. 1) in our galaxy sample with velocities between 1240 and 1680 km s^{-1} , from which we regard 9 galaxies as group members.

Two lines of sight (LOS) in our COS sample towards NGC 985 and Mrk 1044 pass the NGC 1052 group at normalized impact parameters of $\rho_{\text{GC}}/R_{\text{vir}} = 1.24$ and 2.04 from the group's center (GC) position. HI Ly α absorption is detected within the group's radial velocity range along both sightlines (see Fig. 2). Very weak ($< 30 \text{ m\AA}$) but significant single-component Ly α absorption is detected at 1457 km s^{-1} (NGC 985) and 1433 km s^{-1} (Mrk 1044). Following our definition in Sect. 2.3, these absorbers define a coherent absorption pattern along these neighboring sightlines that are separated by 38 kpc at the distance of the NGC 1052 group. These two sightlines do not pass the CGM of any of the galaxies in this field (including group member galaxies and field galaxies). The S/N per resolution element in these two spectra is ≥ 50 , thus very high. Because of the weakness

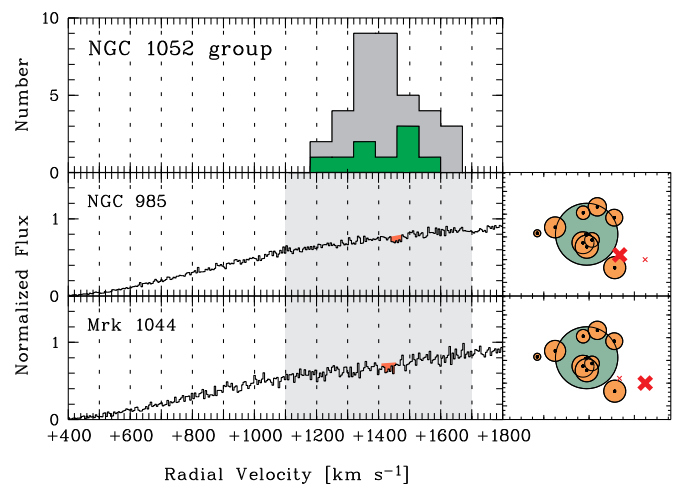


Fig. 2. Velocity plots for HI Ly α absorption for the sightlines passing the outer environment of the NGC 1052 group (lower two panels). OGrM absorbers are marked in dark orange. The expected radial velocity range for OGrM absorption is indicated with the gray-shaded area (see Sect. 2.3). The upper panel shows the velocity distribution for group member galaxies (green histogram) and for all galaxies in the group's field (gray histogram).

of these absorption features, we re-analyzed the two original data sets with an alternative version of the CALCOS sightline, as recently developed in our group for the purpose of analyzing He II Ly α transmission spikes (Makan et al., 2021). These features remain, however, clearly present also in the newly reduced data set with almost no changes in the

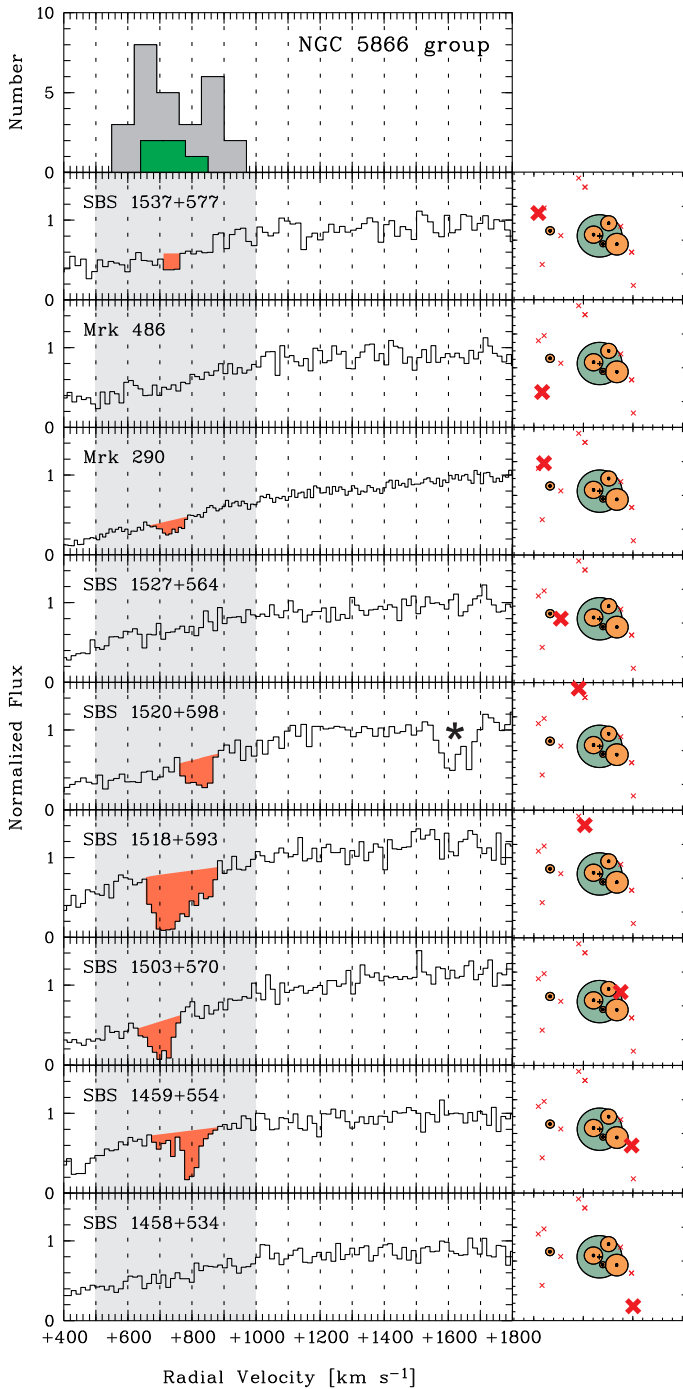


Fig. 3. Same as Fig. 2, but for the NGC 5866 group. Absorption lines not related to the OGrM or CGM of member/field galaxies are labeled with the star symbol.

flux distribution, leading us to conclude that they represent real intervening absorption features that trace the OGrM of the NGC 1052 group.

With column densities of $\log N(\text{H I}) = 12.75$ (Mrk 1044) and 12.50 (NGC 985), these absorbers represent the weakest systems in our OGrM sample. Note that such weak systems would remain unnoticed in COS spectra with $S/N < 30$, thus in most archival AGN data sets.

3.3. NGC 5866 group

The NGC 5866 group field is relatively sparse with only 27 galaxies in the range $\alpha_{2000} \approx 237 - 220$ deg, $\delta_{2000} \approx 53 - 60$ deg at velocities $v = 560 - 960$ km s⁻¹, from which 5 galaxies are regarded as secure group members. The group's velocity dispersion ($\sigma_{\text{gr}} = 82$ km s⁻¹) and total luminosity are small, resulting in a rather small group mass and virial radius (see Table 1).

The large-scale environment of the NGC 5866 group at $\rho_{\text{GC}}/R_{\text{vir}} = 1 - 3$ is sampled by nine AGN sightlines that are not contaminated by CGM absorption (see Sect. 2.3). The normalized impact parameters range from 1.04 to 2.94. The COS spectral data are of partly good, partly mediocre quality with a S/N for most spectra of ≤ 15 (see Table 2). The majority of the sightlines (6/9) are located in the eastern region of the group (Fig. 1). Significant OGrM Ly α absorption in this velocity range is detected along six sightlines, forming a coherent OGrM absorption pattern (see definition in Sect. 2.3 and velocity plots in Fig. 3). The absorption velocities scatter around ~ 800 km s⁻¹.

The two relatively strong and broad absorbers towards SBS 1518+593 and SBS 1459+554 have an asymmetrical shape, which can be modeled by a two-component structure (Table 3). However, no associated metal absorption is detected in these systems, same as for the other seven OGrM absorbers in the NGC 5866 group environment. The derived H I column densities for OGrM systems around the NGC 5866 group are between $\log N(\text{H I}) = 13.06$ and 14.16 (see Table 3), thus substantially higher than for the NGC 1052 group.

We note that the NGC 5866 group environment and the Ly α absorbers discussed here were also included in the study of Wakker et al. (2015) and identified as filament absorbers. This is no contradiction to our results, as OGrM absorbers (as defined in Sect. 1) represent a sub-class of filament absorbers that are spatially and kinematically coupled to knots in the Cosmic Web (i.e., to groups).

3.4. NGC 4631 group

The NGC 4631 group field ($\alpha_{2000} \approx 198 - 177$ deg, $\delta_{2000} \approx 24 - 37$ deg) is densely populated with 114 galaxies in the velocity range between 430 and 1030 km s⁻¹. From these, however, only 12 galaxies are regarded to be secure members of the NGC 4631 group (Fouqué et al., 1992).

There are 15 sightlines in our AGN sample that pass the outer region of the NGC 4631 group beyond its virial radius at normalized impact parameters between $\rho_{\text{GC}}/R_{\text{vir}} = 1.02$ and 2.77 and at medium to low S/N (see Tables 2 and 3). Six of these sightlines sample the eastern part of the group at right ascensions > 192 deg, while the remaining nine sightlines cluster in the south-western region of the group.

Only along five out of the 15 sightlines is OGrM Ly α absorption detected, implying an OGrM detection rate that is substantially smaller than in the other three groups. The absorption velocities range between ~ 700 and ~ 1100 km s⁻¹, while the equivalent widths have values between 85 and 433 mÅ (see Table 3 and velocity plots in Fig. 4).

The OGrM absorber towards Ton 133 is the only OGrM system in our sample that potentially shows associated metal absorption (here: Si III $\lambda 1206.5$). Since no other metal lines are detected, however, the identification of the Si III absorption remains ambiguous. The very broad ($b = 53$

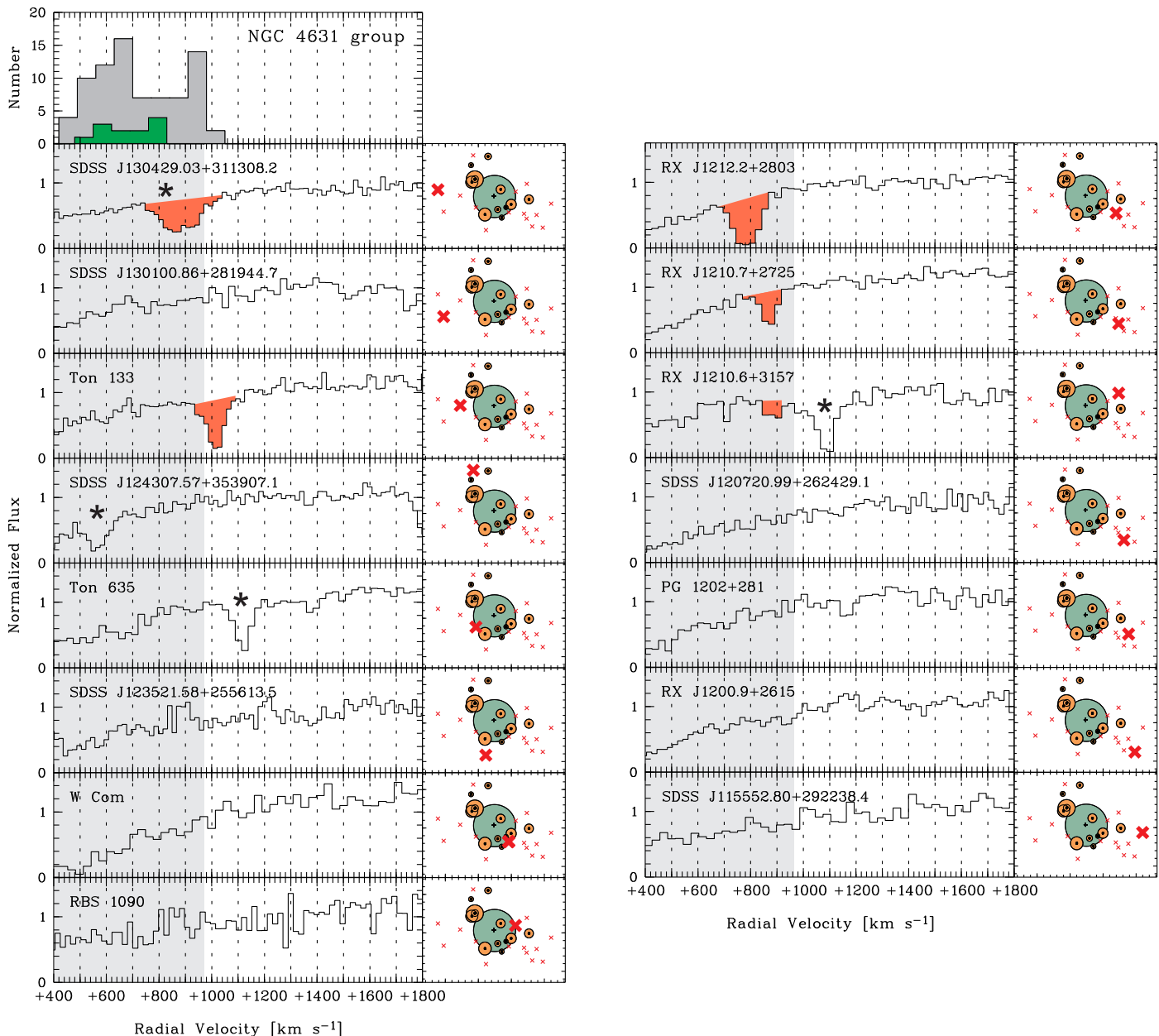


Fig. 4. Same as Fig. 2, but for the NGC 4631 group.

km s^{-1}) OGrM absorber towards the neighboring sightline SDSS J130429.03+311308.2 is potentially blended in the blue wing with intervening C III $\lambda 977.0$ absorption at $z_{\text{abs}} = 0.2477$.

Following our definition in Sect. 2.3, these two absorbers form a coherent OGrM absorption pattern in the eastern part of the group, while the three absorbers along the neighboring sightlines towards RX J1212.2+2803, RX J1210.7+2725, and RX J1210.6+3157 form another coherent OGrM pattern in the south-western part of the NGC 4631 group outskirts.

Note that the immediate environment of NGC 4631 itself is characterized by a gigantic tidal gas stream that stems from the interaction of NGC 4631 with its neighboring galaxies (see Richter et al., 2018, their Fig. 2).

3.5. NGC 3992 group

The relatively large and well-populated NGC 3992 group field ($\alpha_{2000} \approx 188 - 167$ deg, $\delta_{2000} \approx 49 - 59$ deg) contains 236 galaxies at $v = 590 - 1430$ km s^{-1} , 32 of these are regarded as members of the NGC 3992 group.

Seven of the nine selected sightlines for this group pass the western outer environment of the NGC 3992 group at impact parameters between $\rho_{\text{GC}}/R_{\text{vir}} = 1.77$ and 2.77 (see Table 3). They sample an outer region of the group that still contains several massive galaxies (see Fig. 1). Six of these seven sightlines exhibit moderate to strong OGrM Ly α absorption in a coherent absorption pattern near 700 km s^{-1} with Ly α equivalent widths between 131 and 342 mÅ and column densities in the range $\log N(\text{H I}) = 13.53 - 14.14$.

Table 3. Summary of absorption-line measurements

| Group name | LOS No. | Sightline | v_{abs} | $W_{\text{Ly}\alpha}$ | $\log N(\text{H I})$ | $b(\text{H I})$ | $\rho_{\text{GC}}/R_{\text{vir}}^{\text{a}}$ | d_N^{b} |
|------------|----------|--------------------------|------------------------|--------------------------|----------------------|------------------------|--|------------------|
| | | | [km s^{-1}] | [$\text{m}\text{\AA}$] | | [km s^{-1}] | | |
| NGC 1052 | 1 | NGC 985 | 1457 | 17 ± 5 | 12.50 ± 0.09 | 19 ± 5 | 1.24 | 38 |
| | 2 | Mrk 1044 | 1433 | 27 ± 8 | 12.75 ± 0.14 | 32 ± 12 | 2.04 | 38 |
| NGC 5866 | 3 | SBS 1537+577 | 735 | 59 ± 14 | 13.06 ± 0.15 | 16 ± 6 | 2.89 | 12 |
| | 4 | Mrk 486 | ... | ≤ 48 | ≤ 12.95 | ... | 2.94 | ... |
| | 5 | Mrk 290 | 735 | 129 ± 10 | 13.47 ± 0.04 | 42 ± 4 | 2.75 | 12 |
| | 6 | SBS 1527+564 | ... | ≤ 50 | ≤ 12.96 | ... | 1.73 | ... |
| | 7 | SBS 1520+598 | 831 | 168 ± 22 | 13.63 ± 0.07 | 44 ± 7 | 2.86 | 17 |
| | 8 | SBS 1518+593 | 725 | 505 ± 24 | 14.16 ± 0.05 | 43 ± 6 | 2.38 | 17 |
| | | | 826 | | 13.49 ± 0.08 | 43 ± 7 | | .. |
| | 9 | SBS 1503+570 | 703 | 284 ± 25 | 13.96 ± 0.15 | 35 ± 8 | 1.04 | 46 |
| | 10 | SBS 1459+554 | 721 | 228 ± 28 | 13.07 ± 0.13 | 37 ± 13 | 1.64 | 46 |
| | | | 791 | | 13.71 ± 0.06 | 22 ± 4 | | ... |
| | 11 | SBS 1458+534 | ... | ≤ 51 | ≤ 12.97 | ... | 2.81 | ... |
| NGC 4631 | 12 | SDSS J130429.03+311308.2 | 923 | 433 ± 34 | 13.85 ± 0.11 | 53 ± 11 | 2.67 | 47 |
| | 13 | SDSS J130100.86+281944.7 | ... | ≤ 46 | ≤ 12.93 | ... | 2.53 | ... |
| | 14 | Ton 133 | 1013 | 272 ± 22 | 13.92 ± 0.05 | 35 ± 05 | 1.61 | 47 |
| | 15 | SDSS J124307.57+353907.1 | ... | ≤ 28 | ≤ 12.71 | ... | 2.15 | ... |
| | 16 | Ton 635 | ... | ≤ 46 | ≤ 12.93 | ... | 1.02 | ... |
| | 17 | SDSS J123521.58+255613.5 | ... | ≤ 53 | ≤ 12.99 | ... | 1.66 | ... |
| | 18 | WCom | ... | ≤ 85 | ≤ 13.19 | ... | 1.06 | ... |
| | 19 | RBS 1090 | ... | ≤ 102 | ≤ 13.27 | ... | 1.06 | ... |
| | 20 | RX J1212.2+2803 | 788 | 425 ± 20 | 14.34 ± 0.08 | 40 ± 4 | 1.68 | 11 |
| | 21 | RX J1210.7+2725 | 883 | 151 ± 15 | 13.58 ± 0.05 | 25 ± 4 | 1.91 | 11 |
| | 22 | RX J1210.6+3157 | 895 | 85 ± 27 | 13.45 ± 0.22 | 36 ± 9 | 1.66 | 61 |
| | 23 | SDSS J120720.99+262429.1 | ... | ≤ 49 | ≤ 12.95 | ... | 2.36 | ... |
| | 24 | PG 1202+281 | ... | ≤ 51 | ≤ 12.97 | ... | 2.25 | ... |
| | 25 | RX J1200.9+2615 | ... | ≤ 39 | ≤ 12.86 | ... | 2.81 | ... |
| | 26 | SDSS J115552.80+292238.4 | ... | ≤ 49 | ≤ 12.95 | ... | 2.77 | ... |
| | NGC 3992 | 27 | SBS 1213+549 | ... | ≤ 39 | ≤ 12.86 | ... | 1.92 |
| 28 | | SDSS J120506.35+563330.9 | ... | ≤ 79 | ≤ 13.16 | ... | 1.77 | ... |
| 29 | | Mrk 1447 | 772 | 342 ± 22 | 14.14 ± 0.08 | 37 ± 4 | 2.44 | 92 |
| 30 | | SDSS J112448.29+531818.8 | 658 | 285 ± 42 | 13.86 ± 0.05 | 43 ± 5 | 1.80 | 38 |
| 31 | | HS 1119+5812 | ... | ≤ 60 | ≤ 13.04 | ... | 2.77 | ... |
| 32 | | SBS 1116+523 | 723 | 250 ± 18 | 13.86 ± 0.04 | 40 ± 4 | 2.31 | 19 |
| 33 | | SBS 1116+518 | 715 | 220 ± 59 | 13.68 ± 0.08 | 53 ± 12 | 2.43 | 19 |
| 34 | | RX J1117.6+5301 | 676 | 268 ± 31 | 13.87 ± 0.05 | 37 ± 5 | 2.55 | 16 |
| 35 | | SDSS J111443.65+525834.2 | 675 | 131 ± 36 | 13.53 ± 0.11 | 80 ± 23 | 2.34 | 16 |

^a R_{vir} -normalized impact parameter to group center.

^b Distance to neighboring OGrM sightline.

The two sightlines towards SBS 1213+549 and SDSS J120506.35+563330.9 in the eastern region at $\alpha_{2000} > 180$ deg do not show any significant Ly α absorption in the velocity range of the NGC 3992 group.

4. Nature and origin of the OGrM absorbers

4.1. Observational trends

With a detection rate of ~ 50 percent in our survey, kinematically aligned OGrM Ly α absorbers appear to represent a typical absorber class in the outer regions of nearby galaxy groups, where these connect with the ambient Cosmic Web. Per definition, OGrM Ly α absorbers are kinematically aligned with their host groups to ensure that they trace the same overall cosmological environment. But what does this alignment tell us about the nature of these systems?

On the one hand, the coherence in velocity along multiple sightlines could indicate that OGrM absorbers trace the same physical structure (i.e., one and the same “cloud”) probed at different locations, that (for instance) is floating

from the Cosmic Web towards the group center (scenario I). On the other hand, the absorbers may represent independent gas structures (tracing density peaks) that move (“swarm-like”) as an ensemble of clouds within the group’s outer potential well (scenario II). Depending on the actual physical size and the separation between the sightlines at the distances of the groups, one could also think of a combination of both of these scenarios.

To visualize the geometrical setup, we have plotted in Fig. 6 the positions of the OGrM absorbers with respect to the confirmed group member galaxies in 2D and 3D projections (with the velocity as third dimension). The dashed line indicates for each LOS the nearest neighboring sightline that also hosts an OGrM absorber. The linear distance to the nearest neighboring OGrM sightline, d_N , as calculated from the angular separation of the LOS and the group distance, is listed for each OGrM absorber in the last column of Table 3. As can be seen, values for d_N range from 11 to 92 kpc, a linear scale in which both scenarios mentioned above appear realistic. We will elaborate further on the absorber sizes in Sect. 4.4.

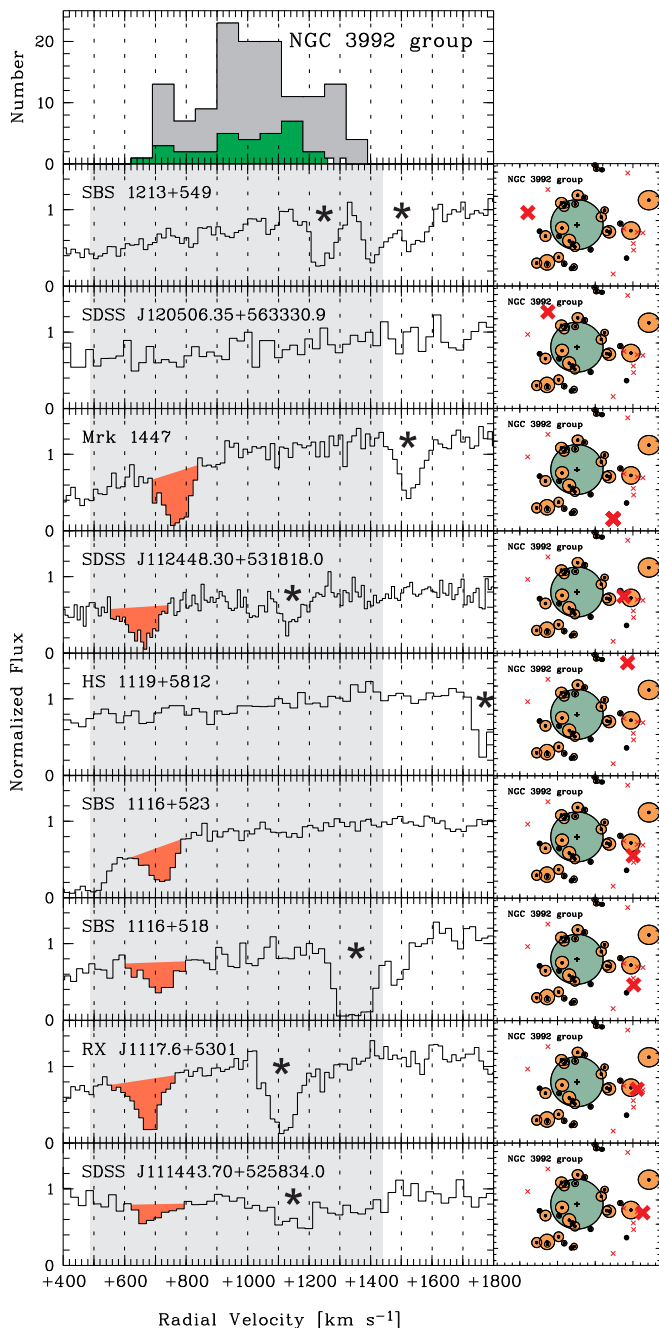


Fig. 5. Same as Fig. 2, but for the NGC 3992 group.

In Fig. 7, we plot the measured Ly α equivalent widths and the derived HI column densities against the normalized absorber impact parameter to the group center. For the entire impact parameter range ($\rho/R_{\text{vir}} = 1 - 3$), there is a lot of scatter with no obvious trend. In future studies of the OGrM, using a larger absorber sample, it would be interesting to also systematically explore the range $\rho/R_{\text{vir}} > 3$ to search for observational trends that may (or may not) indicate a change in the physical conditions of the absorbers related to the decreasing cosmological matter overdensity in this interface region between collapsed group structures and the ambient Cosmic Web.

The overall distribution of HI column densities (lower right panel in Fig. 7) and the median value for $\log N(\text{HI})$ of

13.68 are very similar to those derived for low-redshift IGM filaments (Bouma, Richter & Wendt, 2022; Wakker et al., 2015) or in “blind” Ly α -forest surveys (Lehner et al., 2007; Danforth et al., 2016), implying that the average physical conditions are comparable. This is not really surprising, however, as OGrM absorbers represent a sub-class of the overall intergalactic Ly α population and thus are included in the forementioned surveys.

To explore in more detail the origin and physical conditions of the OGrM systems, one would like to know about the ionization conditions and gas densities in the absorbers, from which one also could derive a characteristic size. With HI Ly α absorption as the only information carrier for all but one of the absorbers, however, we have only a very limited diagnostic toolkit at hand to explore the physical conditions in the gas. Note that the lack of metal-line absorption in our sample of OGrM systems does not necessarily point toward a low metallicity of the OGrM, but rather is a result of the low gas column- and volume densities and the high degree of ionization, which is typical for intergalactic gas at such small cosmological overdensities (e.g. Martizzi et al., 2019, see also Sect. 4.3).

The directly measured quantities available for all OGrM absorbers in our sample are: HI column density, Doppler parameter, radial velocity, and the component structure. From these parameters alone, we can derive estimates for the gas densities, total gas column densities, and absorber sizes only using certain assumptions (Sect. 4.3).

In principle, the measured b value in each absorber provides an upper temperature limit for the gas, as the thermal component of the Doppler parameter can be written as $b_{\text{th}}^2 = 2kT/m_{\text{H}}$, with m_{H} being the mass of the hydrogen atom. It is, however, commonly assumed that the observed b value is composed of a thermal and a non-thermal component, so that $b^2 = b_{\text{th}}^2 + b_{\text{non-th}}^2$. In our sample, the limited S/N and relatively low spectral resolution complicates the interpretation of the measured HI b values as temperature indicator because the component sub-structure may not be fully resolved. The measured b values in the OGrM absorber-components are all $\leq 53 \text{ km s}^{-1}$ (see Table 3), with only one exception (the weak OGrM absorber towards SDSS J111443.65+525834.2, for which b is only poorly constrained; see last row in Table 3). A value of $b = 53 \text{ km s}^{-1}$ translates into an upper temperature limit of $T \leq 1.7 \times 10^5 \text{ K}$. This value is an order of magnitude lower than the expected virial temperatures of the groups ($T > 4 \times 10^6 \text{ K}$) and lower than what is expected for (equilibrium) collisional ionization to be dominant ($T > 2 \times 10^5 \text{ K}$; Richter et al., 2008). While we cannot exclude that non-equilibrium collisional ionization (e.g., Gnat & Sternberg, 2007) and/or a mixture of collisional and photo-ionization are relevant, the moderate b values for the majority of the systems suggest that the OGrM absorbers are predominantly photoionized (possibly being embedded in a hotter, collisionally ionized gas phase).

4.2. On the incidence rate of OGrM absorbers

The Ly α line density in an AGN spectrum usually is represented by dN/dz , the number of Ly α absorbers per unit redshift, which characterizes the frequency and distribution of gas clouds in the Cosmic Web along that line of sight. The values for dN/dz in “blind” $z \approx 0$ Ly α surveys, where dz is

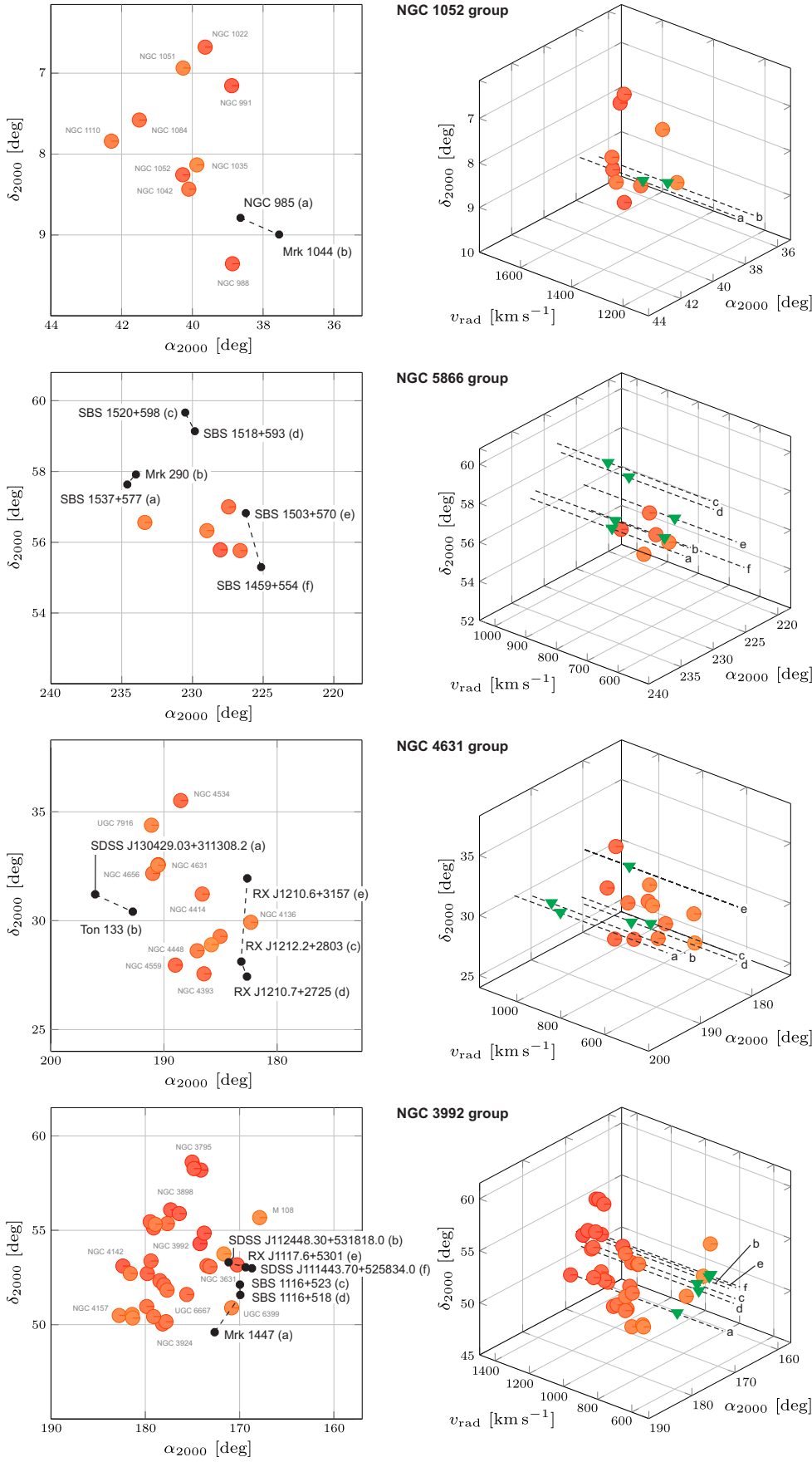


Fig. 6. Spatial configuration of the group member galaxies and the AGN sightlines for the four groups in our sample together with supplementary information. The left panel shows the projected position of group-member galaxies (orange dots) and the AGN sightlines along which OGrM absorption has been detected (black dots). The AGN names are labeled in black, the most important group member galaxies are labeled in gray. The right panel shows the group-member galaxies (orange dots) and the OGrM systems (green triangles) in a 3D position-velocity diagram.

calculated from the redshift paths for multiple AGN sightlines, range from $dN/dz \approx 80$ to 100 for $\log N(\text{H I}) \geq 13.2$

(Danforth et al., 2016; Lehner et al., 2007). Because $v = cz$ at $z \approx 0$, a value of $dN/dz = 100$ for $\log N(\text{H I}) \geq 13.2$

implies that one expects - on average - one Ly α absorber per 3000 km s⁻¹ wide velocity interval (above that column-density level).

Ly α lines are not randomly distributed in redshift space, however, as they follow the small- and large-scale matter distribution (i.e., galaxies, filaments, groups, clusters) in the Cosmic Web (e.g. Morris et al., 1993). The positions of Ly α lines along a AGN spectrum thus are determined by both the cosmological expansion and the peculiar gas motions within collapsed structures. Strong absorbers with $\log N(\text{HI}) \geq 15$ appear to be highly correlated with individual galaxies (e.g. Prochaska et al., 2011), while weaker systems tend to partly cluster in filaments (Bouma, Richter & Wendt, 2022) or partly are part of a population of “random” Ly α absorbers that reside in under-dense regions (Tejos et al., 2012). Bouma, Richter & Wendt (2022) derived for their sample of velocity-selected Ly α absorbers within $z = 0$ filaments an incidence rate of $dN/dz = 189 \pm 25$ for $\log N(\text{HI}) \geq 13.2$. This is substantially higher than for the overall (unselected) Ly α population, reflecting the clustering of Ly α absorbers in cosmological filaments.

To compare the incidence rate of OGrM absorbers with that of filament absorbers and the overall Ly α forest, we follow the same approach as in Bouma, Richter & Wendt (2022) and transform the observed OGrM detection rate into a dN/dz value. The total OGrM absorption path length in our sample (in velocity units) is given by

$$\Delta v_{\text{OGrM}} = \sum_{i=1}^4 \mathcal{N}_{13.2,i} f_i \Delta v_i, \quad (4)$$

where i is the index for our 4 groups, $\mathcal{N}_{13.2,i}$ is the number of sightlines per group that have sufficient S/N to detect OGrM Ly α absorption at $\log N(\text{HI}) \geq 13.2$, $f_i \leq 1$ is a factor that corrects for line blends, and Δv_i is the expected velocity range for OGrM absorption in group i , as defined in Sect. 2.3. Since we have rigorously sorted out sightlines that are contaminated by CGM absorption within Δv_i , we can safely set $f_i = 1$.

Based on equation (4), the total OGrM velocity path in our sample comes out to $\Delta v_{\text{OGrM}} = 20,650$ km s⁻¹. Because $v = cz$ at $z = 0$, this velocity range corresponds to an OGrM redshift pathlength of $dz = \Delta v_{\text{OGrM}}/c = 0.06888$. Note that the OGrM redshift pathlength calculated in this way has no cosmological meaning; it just indicates the integrated velocity range for OGrM absorption in our AGN sample in unit redshift ($\Delta v/c$). Having 16 OGrM absorbers at $\rho/R_{\text{vir}} = 1 - 3$ with $\log N(\text{HI}) \geq 13.2$, we thus derive $dN/dz = 16/0.06888 = 232 \pm 58$. This is more than twice the number density in the overall Ly α forest ($dN/dz = 80 - 100$) and ~ 25 percent above the value for $z = 0$ filaments (189; see above).

Our study therefore indicates that the outer regions of groups at $\rho/R_{\text{vir}} = 1 - 3$ are characterized by an overdensity of Ly α absorbers when compared to other regions in the local Cosmic Web. The high value for dN/dz in the OGrM needs to be, however, re-evaluated and confirmed by a larger group/absorber sample.

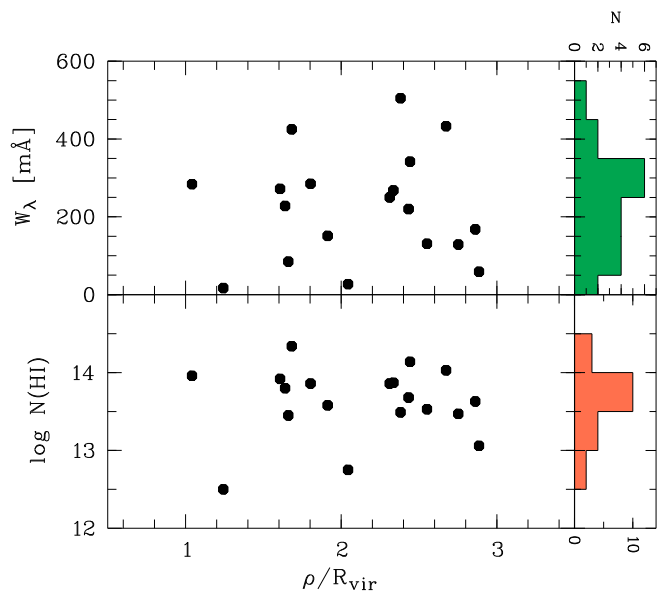


Fig. 7. The Ly α equivalent widths and logarithmic HI column densities of OGrM absorbers are plotted against the relative absorber impact parameter to the group center. No clear trend can be seen in these plots.

4.3. Hydrostatic model

To shed more light into the physical conditions of the OGrM absorber population, we discuss a simple hydrostatic toy model, in which we regard the absorbers as mildly overdense gas patches that have neutral gas fractions high enough to be detectable in HI Ly α absorption and that are photoionized by the cosmic UV background. The fundamental assumption in this model is that the absorbing structures stay roughly in pressure equilibrium with their ambient gaseous environment and that the gas is in hydrostatic equilibrium, gravitationally confined by the underlying matter distribution.

We are aware of the fact that such a model represents a rather over-idealized approach, as the assumption of hydrostatic equilibrium may not hold for gas in the outskirts of low-mass galaxy groups (Paul et al., 2017). However, in the absence of any alternative, more reliable approach, we are interested to explore the outcome of such a model to get a general idea of realistic absorber densities and sizes that we then can relate to the observed OGrM absorption pattern and the angular separation between the sightlines.

We start our model description with the DM mass distribution within $3R_{\text{vir}}$ of the group centers, which we assume to follow a NFW profile (see also Sect. 2.2). Using the formalism described in Richter (2020), we calculate the expected radial gas pressure profiles of the gas bound to the groups within $3R_{\text{vir}}$ as a function of the groups’ total masses, M_L (see Table 1). If we further assume that the projected distances of the absorbers to the group centers (i.e., the impact parameters) are equal to the actual radial distances, R , we can obtain in this way an estimate for P/k for each absorber. The resulting values are listed in Table 4, fourth row. With the thermal pressure being $P/k = n_{\text{H}}T$, ignoring non-thermal pressure components as well as assuming an upper temperature limit of $\log T = 4.5$ for photoionized gas, we then obtain a lower limit for n_{H}

for each absorber from this model. The results for n_{H} are shown in Table 4, sixth row. The values that we obtain from this approach vary from $\log n_{\text{H}} = -5.00$ to -3.72 , a density range that is characteristic of intergalactic/intra-group environments and the Ly α forest, as seen in hydrodynamical cosmological simulations (Martizzi et al., 2019). A direct consequence of our hydrostatic group model with constant T is that n_{H} (such as P/k) decreases quickly with increasing distance R from the group center with a trend depending on the total group mass (Richter, 2020, their equation A.12). This trend is shown for all four groups in Fig. B.1 in the Appendix.

In our model, we regard photoionization by the cosmic UV background as the only relevant ionization process to ionize hydrogen in the OGrM absorbers. This is motivated by the fact that the OGrM absorbers are far away from any local ionization sources (such as AGN or stars) and is supported by the temperature limits from the measured b values (see above). We adopt a photoionization rate of $\Gamma = 7 \times 10^{-14} \text{ s}^{-1}$ for the $z = 0$ IGM, based on the results from Fumagalli et al. (2017). In analogy to HI absorbers in the $z = 0$ Ly α forest, we then can estimate the neutral gas fraction, f_{HI} , in the absorbers assuming photoionization equilibrium and using the simple relation

$$f_{\text{HI}} = 5.3 n_{\text{H}} T_4^{-0.76}, \quad (5)$$

where T_4 is the gas temperature in units 10^4 K (see, e.g., Richter et al., 2008, and discussion therein). The temperature term in this equation reflects the temperature dependence of the hydrogen recombination coefficient. Since our model provides lower limits for $\log n_{\text{H}}$ at a constant value of $T_4 = 3$, we likewise obtain lower limits for f_{HI} (Table 4, eighth column) and upper limits for the total hydrogen column density, $N(\text{H}) = N(\text{HI}) + N(\text{HII}) = N(\text{HI})/f_{\text{HI}}$ (Table 4, seventh column). Finally, from the relation $L = N(\text{H})/n_{\text{H}}$, we get an upper limit for the absorption path length L in the absorbers that we can regard as a characteristic length scale for the absorbing structures. The limits for $\log(L/\text{pc})$ are listed in the 9th column of Table 4. These span a large range between 1.09 and 4.83, corresponding to absorber sizes between 12 pc and 68 kpc with a median value of 2.8 kpc. Similarly large ranges in absorber sizes are also found in CGM absorbers, where the ionization conditions can be much more precisely constrained using the various transitions from intermediate and high metal ions and advanced modeling techniques (e.g., Sameer et al., 2024; Richter et al., 2009).

4.4. On the origin and fate of OGrM absorbers

The absorber sizes, L , estimated from our hydrostatic model now can be directly compared with the linear distances between neighboring OGrM sightlines, d_N (Sect. 4.1). In the last column of Table 4, we list the ratio (upper limit) between the absorber size and the distance to the nearest OGrM absorber, L/d_N . Only for four OGrM absorbers in the NGC 5866 group is this ratio clearly < 1 , suggesting that the estimated absorber-size limits are (substantially) smaller than the sightline separations. If (regardless of the simplicity of our modeling) this estimate reflects reality, these numbers would imply that these OGrM Ly α absorbers represent individual gas clumps that follow as a

conglomerate the large-scale motions of matter in the outer regions of the groups' potential wells ("swarm-like", scenario II; see above).

For the remaining majority of the OGrM absorbers, however, the upper limits for L/d_N are all above unity, some of them substantially. For these systems, both scenarios discussed in Sec. 4.1 are possible and it therefore cannot be excluded that the velocity alignment of OGrM absorption along these adjacent sightlines is a result of the fact that the various LOS that sample a coherent OGrM structure pass through the same kpc-scale Ly α cloud.

While it is tempting to calculate an upper limit for the absorber's total gas masses from our simple hydrostatic model to evaluate their contribution to the groups' baryon budget, we refrain from doing so because of the unknown absorber geometry and the very large uncertainties that would come along with such an estimate. Future studies of OGrM absorbers in hydrodynamical cosmological simulations and the analysis of ultra-deep X-ray observations would be of great help to understand i) whether the high incidence rate of OGrM absorbers derived in Sect. 4.2 is a result of AGN feedback, which potentially lifts and retains large amounts of warm/hot gas in the outskirts of galaxy groups (Eckert et al., 2021), or any other large-scale gas-circulation processes, ii) whether the $(1 - 3)R_{\text{vir}}$ range around groups hosts a substantial baryon reservoir, and iii) to what amount the photoionized OGrM absorbers are surrounded by a hotter, collisionally ionized medium. Similarly, hydrodynamical simulations of OGrM absorbers in group environments of different halo masses and evolutionary states will be important to understand the gas dynamics, the importance of OGrM absorbers for the general properties of the IGrM in the group centers, and their fate in their role as baryon carrier to feed the disks of group member galaxies and/or their hot coronal halos with metal-poor gas from the IGM (see Afruni et al., 2023).

5. Summary and conclusions

In this paper, we have studied coherent HI Ly α absorption patterns in the outer-group medium (OGrM) in the outskirts of four nearby ($D \leq 20 \text{ Mpc}$), low-mass galaxy groups (NGC 1052 group, NGC 5866 group, NGC 4631 group, and NGC 3992 group) using archival UV spectral data from HST/COS. For this, we have analyzed Ly α absorption near the groups' systemic velocities along 35 AGN sightlines that i) pass the four groups at normalized impact parameters in the range $\rho/R_{\text{vir}} = 1 - 3$ and ii) are not contaminated by CGM absorption from foreground/group-member galaxies. The main results of our study can be summarized as follows:

(1) Coherent OGrM HI Ly α absorption (Ly α absorption that is measured at similar group radial velocities along ≥ 2 adjacent sightlines) with equivalent widths between $W_\lambda = 17$ and $505 \text{ m}\text{\AA}$ is detected along 19 out of the 35 sightlines. This high detection rate of more than 50 percent indicates that diffuse HI-absorbing gas in the outskirts of galaxy groups has a relatively large absorption-cross section.

(2) From the modeling of the observed Ly α absorption profiles we determine HI column densities and Doppler parameters for the 19 OGrM absorbers. The

Table 4. Modeled physical conditions in the OGrM absorbers

| Group name | LOS No. | Sightline | $\log P/k$ | $\log T$ | $\log n_{\text{H}}$ | $\log N(\text{H})$ | $\log f_{\text{HI}}$ | $\log L$ | L/d_N |
|------------|---------|--------------------------|------------|------------|---------------------|--------------------|----------------------|-------------|---------------|
| NGC 1052 | 1 | NGC 985 | 1.12 | ≤ 4.5 | ≥ -3.72 | ≤ 15.86 | ≥ -3.36 | ≤ 1.09 | ≤ 3106.9 |
| | 2 | Mrk 1044 | 0.50 | ≤ 4.5 | ≥ -4.34 | ≤ 16.72 | ≥ -3.97 | ≤ 2.57 | ≤ 102.7 |
| NGC 5866 | 3 | SBS 1537+577 | -0.16 | ≤ 4.5 | ≥ -5.00 | ≤ 17.69 | ≥ -4.63 | ≤ 4.20 | ≤ 0.8 |
| | 5 | Mrk 290 | -0.11 | ≤ 4.5 | ≥ -4.95 | ≤ 18.05 | ≥ -4.58 | ≤ 4.51 | ≤ 0.4 |
| | 7 | SBS 1520+598 | -0.16 | ≤ 4.5 | ≥ -5.00 | ≤ 18.26 | ≥ -4.63 | ≤ 4.77 | ≤ 0.3 |
| | 8 | SBS 1518+593 | 0.08 | ≤ 4.5 | ≥ -4.76 | ≤ 18.56 | ≥ -4.40 | ≤ 4.83 | ≤ 0.3 |
| | | | 0.08 | ≤ 4.5 | ≥ -4.76 | ≤ 17.89 | ≥ -4.40 | ≤ 4.16 | ≤ 1.2 |
| | 9 | SBS 1503+570 | 1.10 | ≤ 4.5 | ≥ -3.74 | ≤ 17.34 | ≥ -3.38 | ≤ 2.59 | ≤ 118.0 |
| 10 | | SBS 1459+554 | 0.54 | ≤ 4.5 | ≥ -4.30 | ≤ 17.00 | ≥ -3.93 | ≤ 2.81 | ≤ 71.1 |
| NGC 4631 | 12 | SDSS J130429.03+311308.2 | 0.12 | ≤ 4.5 | ≥ -4.72 | ≤ 17.93 | ≥ -4.36 | ≤ 4.16 | ≤ 1.7 |
| | | | 0.12 | ≤ 4.5 | ≥ -4.72 | ≤ 18.21 | ≥ -4.36 | ≤ 4.44 | ≤ 3.2 |
| | 14 | Ton 133 | 0.76 | ≤ 4.5 | ≥ -4.08 | ≤ 17.64 | ≥ -3.72 | ≤ 3.23 | ≤ 27.6 |
| | 20 | RX J1212.2+2803 | 0.70 | ≤ 4.5 | ≥ -4.14 | ≤ 18.11 | ≥ -3.77 | ≤ 3.76 | ≤ 1.9 |
| | 21 | RX J1210.7+2725 | 0.54 | ≤ 4.5 | ≥ -4.30 | ≤ 17.51 | ≥ -3.93 | ≤ 3.32 | ≤ 5.2 |
| | 22 | RX J1210.6+3157 | 0.72 | ≤ 4.5 | ≥ -4.12 | ≤ 17.20 | ≥ -3.75 | ≤ 2.83 | ≤ 89.7 |
| NGC 3992 | 29 | Mrk 1447 | 0.68 | ≤ 4.5 | ≥ -4.16 | ≤ 17.93 | ≥ -3.79 | ≤ 3.60 | ≤ 23.3 |
| | 30 | SDSS J112448.29+531818.8 | 1.06 | ≤ 4.5 | ≥ -3.78 | ≤ 17.27 | ≥ -3.41 | ≤ 2.56 | ≤ 104.3 |
| | 32 | SBS 1116+523 | 0.75 | ≤ 4.5 | ≥ -4.09 | ≤ 17.58 | ≥ -3.72 | ≤ 3.18 | ≤ 12.4 |
| | 33 | SBS 1116+518 | 0.69 | ≤ 4.5 | ≥ -4.15 | ≤ 17.46 | ≥ -3.78 | ≤ 3.12 | ≤ 14.3 |
| | 34 | RX J1117.6+5301 | 0.74 | ≤ 4.5 | ≥ -4.10 | ≤ 17.60 | ≥ -3.73 | ≤ 3.21 | ≤ 9.9 |
| | 35 | SDSS J111443.65+525834.2 | 0.63 | ≤ 4.5 | ≥ -4.21 | ≤ 17.37 | ≥ -3.85 | ≤ 3.10 | ≤ 12.8 |

Parameters and their units: gas pressure P/k in [cm^{-3} K]; gas temperature T in [K], hydrogen volume density n_{H} in [cm^{-3}], total hydrogen column density $N(\text{H})$ in [cm^{-2}], neutral hydrogen fraction f_{HI} , absorption path length L in [pc].

derived logarithmic HI column densities lie in the range $\log N(\text{HI}) = 12.50 - 14.34$ with a median value of 13.68, thus very similar to the column-density range found in the overall population of Ly α forest absorbers in nearby ($z = 0$) cosmological filaments (Bouma, Richter & Wendt, 2022; Wakker et al., 2015), which the OGrM absorbers are part of. The derived Doppler parameters span a large range ($b = 16 - 80 \text{ km s}^{-1}$), but unresolved velocity structure is likely to be present in many of these lines. In the impact parameter range sampled by our study ($\rho/R_{\text{vir}} = 1 - 3$), we do not find any dependency between the Ly α equivalent width/HI column density and the group impact parameter. Only one OGrM Ly α absorber in our sample possibly has associated metal-line absorption (Si III), while the vast majority of the systems are Ly α -only absorbers.

(3) We use a simple hydrostatic toy model for photoionized gas in the outskirts of galaxy groups to constrain the physical conditions in the observed OGrM absorber population. From this, we obtain lower limits for the gas densities from $\log n_{\text{H}} = -5.00$ to -3.72 , comparable to the density range expected for the Ly α forest. The resulting upper limits for the absorber sizes lie between 12 pc and 68 kpc with a median value of 2.8 kpc. Only for four OGrM absorbers, the estimated size limits are smaller than the linear separation between the adjacent OGrM absorbers in the group, suggesting that these absorbers represent independent gas structures (tracing gas-density peaks) that move as an ensemble within or towards the group's potential well. For the remaining 15 absorbers, no clear statement can be made in this regard.

(4) By converting the observed OGrM Ly α absorption-cross section into an incidence rate, we find that the

number of Ly α absorbers per unit redshift in nearby group environments is $dN/dz = 232 \pm 58$ for absorbers with $N(\text{HI}) \geq 13.2$ and $\rho/R_{\text{vir}} = 1 - 3$. This is ~ 25 percent above the value derived for Ly α absorbers in filaments at $z = 0$ ($dN/dz = 189 \pm 25$; Bouma, Richter & Wendt, 2022) and more than twice the value for the overall $z = 0$ Ly α forest ($dN/dz = 80 - 100$; Danforth et al., 2016; Lehner et al., 2007) considering the same column-density range. The large incidence rate may hint at a substantial reservoir of baryons in the outskirts of galaxy groups in the form of diffuse ionized gas, but future observations and simulations are required to reliably constrain the mass budget in the OGrM and its connection to AGN feedback (Eckert et al., 2021).

Our study of OGrM Ly α absorbers unveils a number of interesting properties of diffuse gas in the outskirts of galaxy groups that deserve to be addressed in a larger absorption-line survey. We are currently undertaking a fully automated analysis of all AGN spectra in the HST/COS archive as part of the QUALSTAR (Quasar Absorption Lines Standardized Automated Recovery) project (Richter, in prep.), from which we will obtain detailed information on N , b , z_{abs} for several thousand Ly α absorbers in the nearby Universe. This information will be directly compared to galaxy data from recent surveys to systematically investigate the connection between Ly α absorbers and their ambient large-scale environment (e.g., filaments, groups, and clusters). In this way, we will pinpoint the gaseous matter distribution in the transition zones between cosmological filaments and knots in the Cosmic Web. The observational data will also be compared with mock spectral data synthesized from hydrodynamical cosmological simulations.

A particularly demanding observational task, yet crucial for a better understanding of gas in group environments, will be a reliable estimate of the total gas mass that is hosted in the outskirts of groups. Such an estimate can only be obtained from a larger OGrM Ly α absorber sample in combination with deep X-ray observations that would trace the hot ($T > 10^6$ K) phase of the OGrM which may carry the bulk of the baryons in this region. Also, a systematic analysis of the kinematics of Ly α absorbers at even larger distances ($\rho/R_{\text{vir}} = 1 - 10$) from the group centers is highly desired to characterize the streaming motion of these gas absorbers towards the group centers and to estimate the contribution of this matter reservoir to the galaxies' gas accretion and star-formation rate.

Acknowledgements. This research has made use of the SIMBAD database, operated at CDS, Strasbourg, France. This research also has made use of the NASA/IPAC Extragalactic Database (NED), which is funded by the National Aeronautics and Space Administration and operated by the California Institute of Technology. The authors would like to thank the anonymous referee for helpful comments and suggestions.

References

- Afruni, A., Pezzulli, G., Fraternali, F., & Gronnow, A. 2023, MNRAS, 524, 2351
- Berlind, A.A., Frieman, J., Weinberg, D.H., et al. 2006, ApJS, 167, 1
- Bielby, R., Crighton, N.H.M., Fumagalli, M., et al. 2017, MNRAS, 468, 1373
- Borthakur, S., Yun, M.S., & Verdes-Montenegro, L. 2010, ApJ, 710, 385
- Bouma, S.J.D., Richter, P. & Wendt, M. 2022, A&A, 647, A166
- Bryan, G., & Norman, M. 1998, ApJ, 495, 80
- Burchett, J.N., Tripp, T.M., Wang, Q.D., Willmer, C.N.A., Bowen, D.V., & Jenkins, E.B. 2018, MNRAS, 475, 2067
- Chen, H.-W., Johnson, S.D., Zahedy, F.S., Rauch, M., & Mulchaey, J.S. 2017, ApJL, 842, L19
- Danforth, C.W., Keeney, B.A., Tilton, E.M., et al. 2016, ApJ, 817, 111
- Debes, J.H., Becker, G. & Roman-Duval, J. 2016, COS Instrument Science Report, 15
- Despali, G., Giocoli, C. & Tormen, G. 2014, MNRAS, 443, 2208
- Dinshaw, N., Weymann, R.J., Impey, C.D., Foltz, C.B., Morris, S.L., & Ake, T. 1997, ApJ, 491, 45
- Eckert, D., Gaspari, M., Gastaldello, F., Le Brun, A.M.C., & O'Sullivan, E. 2021, Universe 7, 142
- Einasto, M., Einasto, J., & Tenjes, P. 2024, A&A 681, A91
- Eke V.R., Baugh C.M., Cole S., Frenk C.S., & Navarro J.F. 2006, MNRAS, 370, 1147
- Fouqué, P., Gourgoulhon, E., Chamaraux, P., Paturel, G. 1992, A&AS, 93, 151
- French, D.M. & Wakker, B.P. 2017, ApJ, 837, 138
- Fumagalli, M., Haardt, F., Theuns, T., et al. 2017, MNRAS, 467, 4802
- Garcia, A.M. 1993, A&AS, 100, 47
- Gnat, O. & Sternberg, A. 2007, ApJS, 168, 213
- Gourgoulhon, E., Chamaraux, P., Fouqué, P. 1992, A&A 255, 69
- Green, J.C., Froning, C.S., Osterman, S., et al. 2012, ApJ, 744, 60
- Lehner, N., Savage, B.D., Richter, P., Sembach, K.R., Tripp, T.M., & Wakker, B.P. 2007, ApJ, 658, 680
- Lovisari L., Ettori S., Gaspari M., Giles P. A., 2021, Universe, 7, 139
- Makan, K., Worseck, G., Davies, F.B., Hennawi, J.F., Prochaska, J.X., & Richter, P. 2021, ApJ, 912, 38
- Maller, A.H. & Bullock, J.S. 2004, MNRAS, 355, 694
- Marini, I., Popesso, P., Dolag, K. et al. 2025, A&A 698, A191
- Morris, S.L., Weymann, R.J., Dressler, A., et al. 1993, ApJ, 419, 524
- Martizzi, D., Vogelsberger, M., Artale, M.C. 2019, MNRAS, 486, 3766
- Mulchaey, J.S., Mushotzky, R.F., Burstein, D., & Davis, D.S. 1996, ApJL, 456, L5
- Mulchaey J.S. 2000, ARA&A, 38, 289
- Muzahid, S., Fonseca, G., Roberts, A., et al. 2018, MNRAS, 476, 4965
- Oppenheimer, B.D., Babul, A., Bahé, Y., Butsky, I.S., & McCarthy, I.G. 2021, Universe, 7, 209
- Osmond, J.P.F. & Ponman, T.J. 2004, MNRAS, 350, 1511
- Navarro J.F., Frenk C.S., & White S.D.M. 1995, MNRAS, 275, 56
- Paul, S., John, R.S., Gupta, P., & Kumar, H. 2017, 471, 2
- Pointon, S.K., Nielsen, N.M., Kacprzak, G.G., et al. 2017, ApJ, 844, 23
- Pointon, S.K., Kacprzak, G.G., Nielsen, N.M., et al. 2020, ApJ, 159, 216
- Prochaska, J.X., Weiner, B., Chen, H.W., Mulchaey, J., & Cooksey, K. 2011, ApJ, 740, 91
- Proctor, R.N., Mendes de Oliveira, C., Azanha, L., Dupke, R., & Overzier, R. 2015, MNRAS, 449, 234
- Richter, P., Paerels, F.B.S., Kaastra, J.S. 2008, SSRv, 134, 25
- Richter, P., Charlton, J.C., Fangano, A.P.M., Ben Bekhti, N., & Masiero, J.R. 2009, ApJ, 695, 1631
- Richter, P., Fox, A. J., Wakker, B. P., et al. 2013, ApJ, 772, 111
- Richter, P., Wakker, B.P., Fechner, C., et al. 2016, A&A, 590, A68
- Richter, P., Nuza, S.E., Fox, A.J., et al. 2017, A&A, 607, A48
- Richter, P.; Winkel, B.; Wakker, B. P. et al. 2018, ApJ, 868, 112
- Richter, P. 2020, ApJ, 892, 33
- Sameer, Charlton, J.C., Kacprzak, G.G., et al. 2022, MNRAS, 510, 5796
- Sameer, Charlton, J.C., Wakker, B.P., et al. 2024, MNRAS, 530, 3827
- Savage, B.D. & Sembach, K.R., 1991, ApJ, 379, 245
- Savage, B.D., Kim, T.-S., Wakker, B.P., Keeney, B., Shull, J.M., Stocke, J.T., & Green, J.C. 2014, ApJS, 212, 8
- Shull, J.M. 2014, ApJ, 784, 142
- Stocke, J.T., Keeney, B.A., Danforth, C.W., et al. 2013, ApJ, 763, 148
- Stocke, J. T., Keeney, B. A., Danforth, C. W., et al. 2014, ApJ, 791, 128
- Stocke, J. T., Keeney, B. A., Danforth, C. W., et al. 2019, ApJS, 240, 15
- Tejos, N., Morris, S.L., Crighton, N.H.M., et al. 2012, MNRAS, 425, 245
- Tempel, E., Tamm, A., & Gramann, M. 2014, 2014, A&A, 566
- Tully, R.B. 1987, ApJ, 321, 280
- Tully, R.B. 2015, AJ, 149, 54
- Wakker, B.P., Hernandez, A.K., French, D.M., Kim, T.-S., Oppenheimer, B.D., & Savage, B.D. 2015, ApJ, 814, 40
- Wolfinger, K., Kilborn, V.A., Ryan-Weber, E.V., & Koribalski, B.S. 2016, PASA, 33, 38
- Yun, M.S., Ho, P.T.P., & Lo, K.Y. 1994, Nature, 372, 530

Appendix A: Continuum and absorber modeling

In Fig. A.1, we show as an example the continuum reconstruction and absorption-line modeling for the OGrM absorber at $v = 1457 \text{ km s}^{-1}$ in the NGC 1052 group towards the background source NGC 985 (Table 3). The overall continuum in this region between 1218 and 1226 Å (red solid line) has been modeled from a multi-component Voigt-profile fit of the interstellar H I Ly α absorption using the `span` code (Richter et al., 2013). The slow rise of the continuum level reflects the extended Lorentzian wing of the interstellar Ly α profile. The weak absorber near 1221.5 Å is Ly α at $v = 1457 \text{ km s}^{-1}$ in the NGC 1052 group, which resides in the wing of the Galactic interstellar Ly α absorption. It has been modeled with a single absorption component with $\log N(\text{H I}) = 12.50$ and $b = 19 \text{ km s}^{-1}$. All the absorbers listed in Table 3 have been modeled using a similar approach (see also Sect. 2.3).

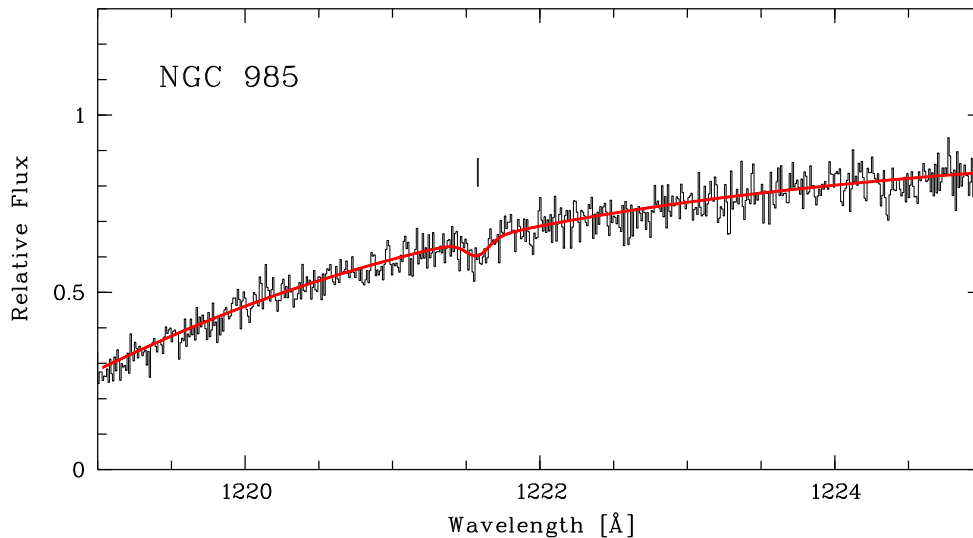


Fig. A.1. Example for the absorption-line modeling of the OGrM absorber towards NGC 985 (see also Table 3).

Appendix B: Radial density distribution in the OGrM absorbers

In Fig. B.1, we show the logarithmic gas density in the OGrM absorbers as a function of the normalized impact parameter to the group center from our hydrostatic toy model (Sect. 4.3). The declining trend for $\log n_{\text{H}}$ is a direct result of the assumed hydrostatic equilibrium, with each group defining its own gravitational potential according to its mass given in Table 1.

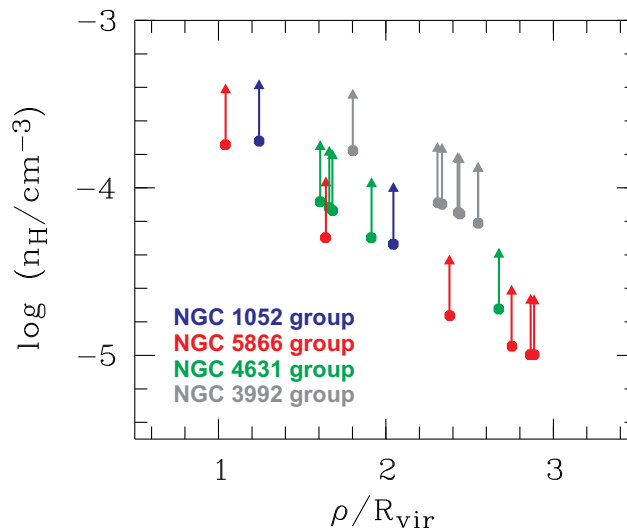


Fig. B.1. Logarithmic gas density in the OGrM absorbers as a function of normalized impact parameter from the hydrostatic toy model (Sect. 4.3).